International Carbon Conference 2018, ICC 2018, 10–14 September 2018, Reykjavik, Iceland

Intercalation of aromatic sulfonates in 'green rust' via ion exchange

Jeffrey Paulo H. Perez[a,b,*,†], Marco C. Mangayayam[c,†], Sandra Navaz Rubio[a,b],
Helen M. Freeman[a], Dominique J. Tobler[c], Liane G. Benning[a,b]

[a]GFZ German Research Center for Geosciences, Telegrafenberg, 14473 Potsdam, Germany
[b]Department of Earth Sciences, Free University of Berlin, 12249 Berlin, Germany
[c]Nano-Science Centre, Department of Chemistry, University of Copenhagen, 2100 Copenhagen, Denmark

Abstract

'Green rust' intercalated with aromatic sulfonates can potentially be effective materials for the treatment of soil and groundwater polluted with chlorinated benzenes. We investigated the potential intercalation of benzene sulfonate (BzS) and 1,3-benzene disulfonate (BzDS) into green rust sulfate (GR_{SO4}) via ion exchange. The GR_{SO4} reacted with various concentrations of sulfonates were characterized by X-ray diffraction, X-ray scattering and transmission electron microscopy. GR interacted with BzDS did not result in intercalation due to stearic hindrance and electrostatic repulsion. For BzS, mixtures of GR_{SO4} and GR-BzS (d_{001} = 14.3 Å) were obtained at molar equivalents of ion exchange capacity >5. The intercalation of BzS in the GR structure is limited (~18% intercalation) since BzS cannot fully replace SO_4^{2-}. The BzS molecules are likely arranged in the interlayer as a dehydrated monolayer with the $-SO_3$ groups facing away in alternate directions.

1. Introduction

'Green rusts' (GRs) are redox-active materials that belong to a family of mixed-valent iron-bearing layered double hydroxides (LDHs) [1, 2]. Similar to LDHs, they are composed of positively charged brucite-like layers of octahedrally coordinated Fe^{II}-Fe^{III} hydroxides that alternate with negatively charged interlayers of anions and water molecules, as well as monovalent cations [3-5]. GRs are usually represented by the general formula, $[Fe^{II}_{(1-x)}Fe^{III}_x(OH)_2]^{x+}[(x/n)\,A^{n-}\cdot mH_2O]^{x-}$, where A^{n-} can be intercalated anions such as Cl^-, CO_3^{2-}, SO_4^{2-}, while x is the molar

* Corresponding author. E-mail address: *jpperez@gfz-potsdam.de*

† Both authors contributed equally in this work.

fraction of Fe^{III}, $[Fe^{III}]/[Fe_{total}]$. Due to their high redox reactivity and excellent surface properties, GRs have been studied for the treatment of toxic metals and organo-halogenated compounds in contaminated soils and groundwaters [3].

In particular, GRs have been examined for the reduction of chlorinated compounds such as chlorinated methanes, ethanes and ethylenes [6-8]. However, the hydrophilic property of GR with inorganic interlayer ions (e.g., Cl^-, CO_3^{2-}, SO_4^{2-}) can decrease its reactivity for chlorinated compounds due to the partitioning of GR in the aqueous phase and chlorinated solvents in the organic phase [8]. This can be resolved by modifying the interlayer region of GRs through the intercalation of amphiphilic organic molecules (hereafter referred to as organo-GRs) – a common approach used in LDHs [9-11]. Such an approach allows chlorinated compounds to partition more easily into the interlayer region, where they become strongly sorbed, enhancing redox reactions with the GR hydroxide layers. This has been demonstrated in previous studies. For example, when GR was intercalated with linear alkyl sulfonates (LAS) via ion-exchange, it adsorbed carbon tetrachloride (CCl_4) more efficiently [12]. GRs modified with linear alkyl carboxylates (LAC) have also shown enhanced reactivity towards reductive dechlorination of carbon tetrachloride (CCl_4) after its sorption of CCl_4 into the organic interlayer [13-15].

In addition to LAS and LAC, intercalation with aromatic sulfonate and carboxylate moieties could also increase the reactivity of GRs, especially for chlorinated benzenes. For Mg-Al LDH compounds, Kameda et al. [16] have shown that benzene sulfonate (BzS) and 1,3-benzene disulfonate (BzDS) can be intercalated into the interlayer. These LDHs intercalated with BzS and BzDS can be selective sorbents for toxic aromatic contaminants due to the resulting π-π interactions between the aromatic rings [17]. Information about how GR phases react with BzS and BzDS is, however, not yet available.

In this study, we provide a proof-of-concept pathway for the synthesis of organo-GRs intercalated with aromatic sulfonates. By harnessing both the enhanced hydrophobicity and redox activity of organo-GRs, GR intercalated with aromatic sulfonates can serve as a 'trap-and-degrade' material for the reductive dechlorination of chlorinated benzenes in contaminated environments. Herein, we examined the intercalation chemistry of BzS and BzDS (Fig. 1) in GR sulfate (GR_{SO4}) via the ion-exchange approach. We characterized the resulting GR samples by X-ray diffraction (XRD) and synchrotron-based pair distribution function (PDF) analysis, combined with transmission electron microscopy (TEM) and analytical spectroscopy to elucidate their crystal structure, morphology and chemical composition.
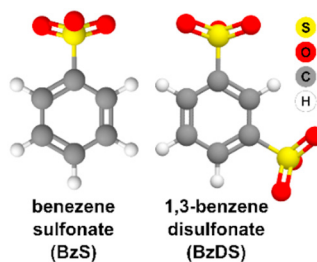

Fig. 1. Structure of aromatic sulfonate precursors.

2. Materials and methods

2.1 General methods

All experimental glass- and plastic-wares were cleaned by soaking them overnight in 5 M HCl and thorough rinsing with Milli-Q water (~18.2 $M\Omega\ cm^{-1}$). All chemicals were ACS reagent grade from VWR and Acros Organics and used without further purification. All stock solutions were prepared from Milli-Q water that was deoxygenated by bubbling O_2-free argon for at least four hours at 100°C. Sample preparation and mineral synthesis were all done at room temperature inside an anaerobic chamber (95% N_2, 5% H_2, Coy Laboratory Products, Inc.) to avoid oxidation of the GR samples.

2.2 Mineral synthesis and ion-exchange

GR$_{SO4}$ was synthesized using the co-precipitation method with slight modification [18]. In brief, 0.3 M Fe(II) and 0.1 M Fe(III) solutions prepared from $(NH_4)_2Fe(SO_4)_2 \cdot 6H_2O$ and $Fe_2(SO_4)_3$ salts were mixed under constant stirring at 350 rpm. The mixed Fe^{II}-Fe^{III} solution was slowly titrated to pH 8 using 0.3 M NaOH, resulting in the precipitation of a blue-green suspension. The suspension was washed several times with O$_2$-free Milli-Q water to remove excess solutes. The amount of formed GR$_{SO4}$ was estimated from the difference between the total iron concentration in the suspension and the dissolved iron concentration in the supernatant (after filtering through 0.2-μm syringe filters). The iron concentrations were analyzed using inductively coupled plasma optical emission spectrometry (ICP-OES). The washed suspension (~11 mM GR$_{SO4}$) was mixed with either a 0.5 M BzS or a 0.25 M BzDS stock solution in headspace crimp bottles to achieve SO$_4^{2-}_{solid}$ to BzS/BzDS$_{aq}$ ratios (molar equivalent of ion exchange capacity) of 1, 2.5, 5, 10 and 20. The mixtures were shaken for seven days at room temperature.

2.3 Mineral characterization

Ambient temperature X-ray diffraction (XRD) patterns were recorded on a Bruker D8 powder diffractometer equipped with a BSI Si(Li) solid detector operating at 40 kV and 40 mA using Cu Kα radiation (λ = 1.5406 Å) with a 0.017° step in the range of Bragg angles 2θ of 5° to 70°. Samples for XRD analysis were loaded on a silicon wafer and the sample holder was sealed using an X-ray transparent cap (Bruker Dome, Polytron) with a low diffusion rate to minimize oxidation.

The local structure of the mineral-end products was investigated using pair distribution function (PDF) analysis. The dry powder samples were placed inside glass capillaries and sealed with paraffin to prevent oxidation during sample transport and measurement. High energy X-ray scattering data were collected at beamline 11-ID-B at Advanced Photon Source, Argonne National Laboratory using a wavelength of 0.2128 Å and a Perkin Elmer amorphous Si 2D detector (40 x 40 cm, placed ~15 cm away from the sample). The set-up geometry was calibrated with Fit-2D using a CeO$_2$ standard powder [19, 20]. Fit-2D was also employed for Lorentz and polarization corrections and azimuthal integration to the 1D spectrum. PDFgetX2 [21] was used to extract PDFs by applying standard corrections including 1D background subtraction (empty glass capillary tubes), incoherent scattering subtractions and corrections for nonlinearity in the detector response. PDFs were obtained from the Fourier transformation of the reduced total scattering structure function, $F(Q)$, using a cutoff of Q_{max} = 24 Å^{-1} to minimize the noise level in the PDFs.

Samples for transmission electron microscopy (TEM) were prepared in an anaerobic chamber by suspending the aromatic sulfonate intercalated GR products in isopropyl alcohol and dropcasting the suspension onto a holey amorphous carbon copper grid. The grid was loaded into a single tilt TEM holder in the anaerobic chamber and sealed for the rapid transfer (< 30 s) into the TEM. Micrographs (TEM) and energy dispersive X-ray spectra (EDX) spectra were recorded using an FEI Tecnai G2 F20 X-Twin FEG TEM operated at 200 kV and equipped with a Gatan Imaging Filter (GIF) Tridiem™, an EDAX X-ray analyzer, and a Fishione HAADF detector. Selected area electron diffraction (SAED) patterns were obtained using an aperture with an effective diameter of 250 nm at the image plane. The stability of the specimens was tested for electron beam damage and no significant changes in the specimens' morphology or crystal structure were observed during data acquisition (10 min per region of interest).

3. Results and discussion

3.1. X-ray diffraction and Rietveld refinement

GR phases typically exhibit sharp and symmetric basal (00*l*) reflections in XRD patterns, which correspond to the interlayer distances between the Fe^{II}-Fe^{III} octahedral hydroxide sheets. In the case of pure GR$_{SO4}$, the most intense (00*l*) reflections are 001 (10. 9 Å), 002 (5.5 Å) and 003 (3.7 Å), with the basal spacing d$_{001}$ composed of the FeO$_6$ octahedral sheet (~4.8 Å) and the interlayer region (6.2 Å) [4, 22].

The XRD patterns of the GR_{SO4} samples interacted with BzDS and BzS are shown in Fig. 2. The similarities between the XRD patterns of pure GR_{SO4} and those interacted with BzDS (Fig. 2a) indicated that BzDS was not intercalated into the GR structure, even at 20 molar equivalents of ion exchange capacity of GR_{SO4}. Anion exchange could have been inhibited by stearic hindrances and electrostatic repulsion during the diffusion of BzDS into the interlayer region [16].
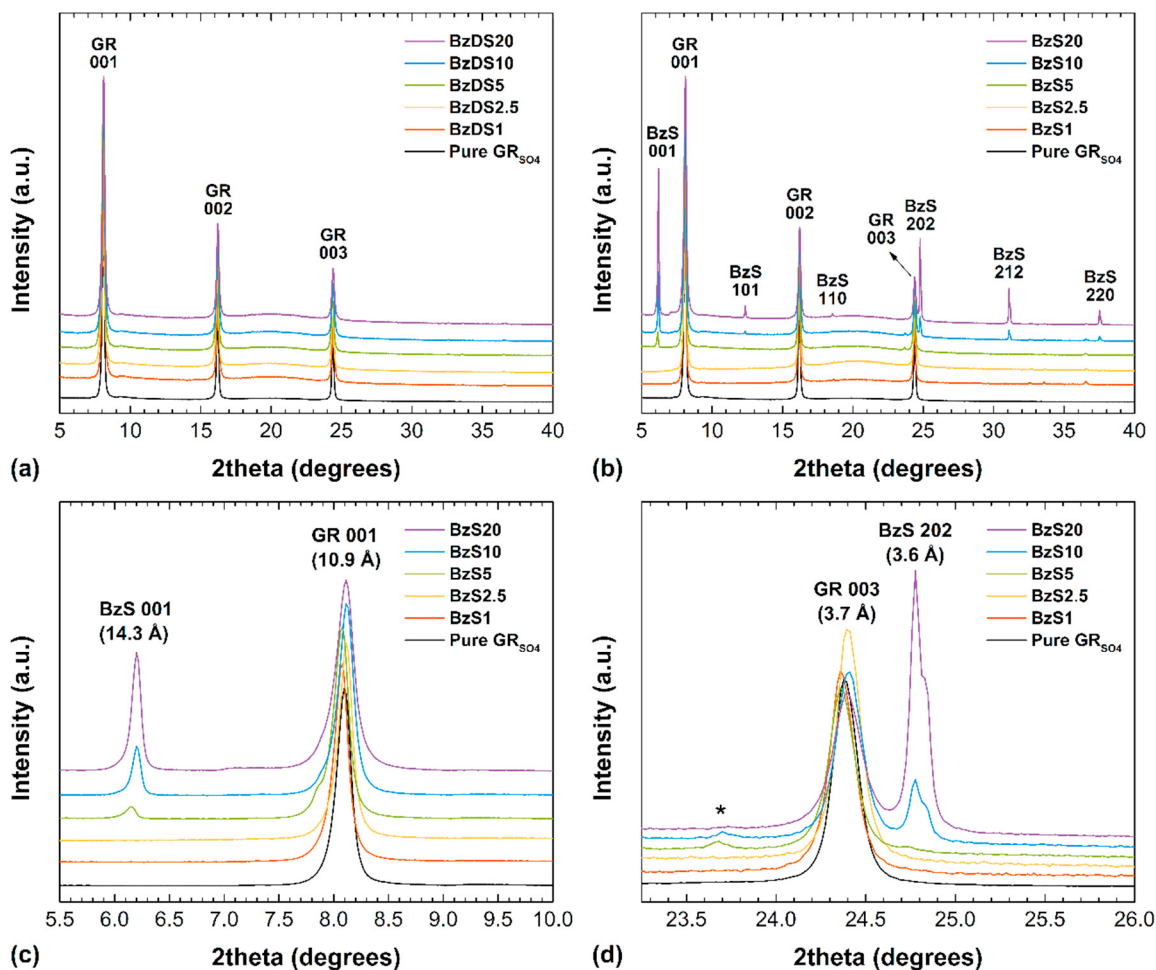

Fig. 2 XRD patterns of resulting GR material after 7 days of reaction with (a) BzDs and (b) BzS. BzS-x or BzDS-x refers to the $SO_4^{2-}_{solid}$ to BzS/BzDS$_{aq}$ ratios of 0 (pure GR_{SO4}), 1, 2.5, 5, 10 and 20. The 2theta ranges in (a) and (b) are clipped from 5 to 40° for clarity. A new set of reflections corresponding to intercalation of BzS in the GR interlayer is observed in (b) BzS reacted GR_{SO4} samples. (c) The GR-BzS 001 peak has a basal spacing of 14.3 Å. (d) The GR-BzS 202 peak has an increased intensity due to the diagonal gliding of the (101) planes. Note: *Cannot be assigned to any GR_{SO4} or GR-BzS calculated reflections.

On the other hand, in the XRD patterns of BzS-interacted GR_{SO4} samples, even at 5-fold molar equivalent, six new (00*l*) reflections can be seen (Fig. 2b). Based on the shape and intensity of these peaks, it may seem like they correspond to two different layered phases with basal spacings of 14.3 Å (Fig. 2c) and 3.6 Å (Fig. 2d). However, the calculated position of the (00*l*) reflections of these two hypothetical phases does not support this. Based on the relationship between their positions, it is likely that all new reflections can be assigned to a single new phase which results from the intercalation of BzS in the interlayer of GR. This intercalation does not occur evenly along the GR sheet which causes a potential diagonal gliding of the layers along the (101) planes of GR (Fig. 3). Hence, three secondary high intensity reflections (> 24.5° 2θ) appeared. Based on a calculated GR-BzS structure, these reflections should be less intense. However, the gliding of the Fe octahedral sheets along the (101) planes (as schematically

indicated in Fig. 3) causes an increase in the intensity of these peaks. A similar case has been reported previously in layered titanates intercalated with monovalent cations [23]. We have indexed the GR-BzS reflections with a modified CIF file of GR_{SO4} from Christiansen et al. [4] to simulate an expansion of the layers without altering the atomic positions. Cell symmetry calculation using the McMaille method [24] confirmed that the structure of the GR-BzS retained the original trigonal symmetry of GR_{SO4}.
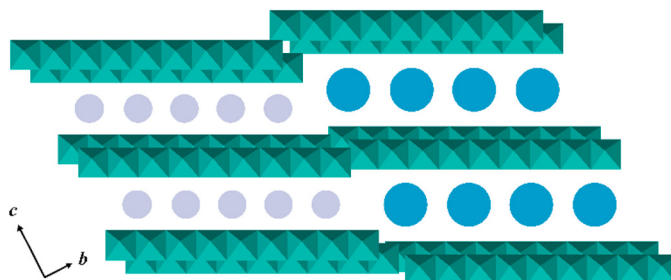

Fig. 3. Schematic diagram of potential diagonal gliding along the (101) planes for mixed phases of GR_{SO4} and GR-BzS. Purple and blue circles represent sulfate and BzS, ions respectively. Modified from Sasaki et al. [23].

With increasing BzS loading, peak intensities increase (Fig. 2b to 2d) and the intercalation efficiency of BzS into the GR_{SO4} structure (Fig. 4a), calculated from the Rietveld refinement of the 001 peak, increases up to 18.1%. This also correlates with the changes in the calculated area of the reflections shown in Fig. 4b. Note that the amount of intercalated BzS does not linearly correlate with the amount of added BzS, and BzS is not able to fully replace SO_4^{2-} in the interlayer. This partial intercalation ultimately results in a heterogeneous arrangement of the BzS interlayer molecules within a single GR particle, which supports and could further explain the observed gliding within the structure.
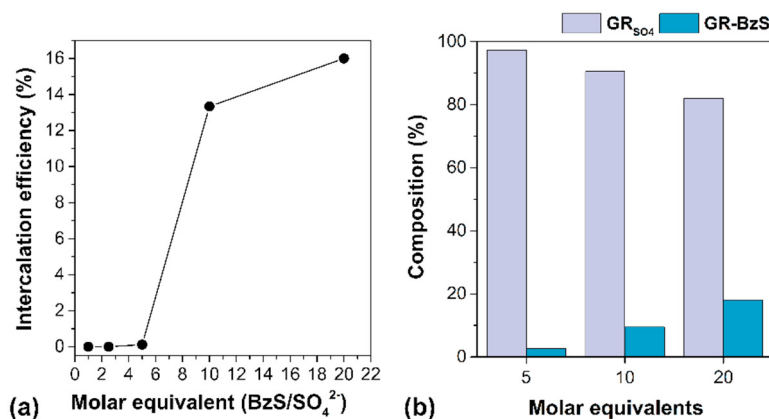

Fig. 4. (a) Intercalation efficiency of BzS calculated from the Rietveld refinement of the 001 peaks of GR_{SO4} and GR-BzS. (b) Composition of BzS-interacted GR_{SO4} based on the calculated areas of the 001 peaks of GR_{SO4} and GR-BzS.

3.2. Pair distribution function analysis

The pair distribution function analysis (PDF) plots in Fig. 5 show the distribution of characteristic atomic distances in the pure GR_{SO4} and the BzS20 interacted GR sample. At first sight, these two PDFs seem very similar, both showing coherent structures up to 80 Å (Fig. 5a). The comparison at the short range shows small differences (Fig. 5b). The GR-BzS20 sample shows a peak at 1.44 Å, which corresponds to the S-O bond in the sulfonate groups of the intercalated BzS molecule. The asymmetric shape of this peak is due to the presence of a second S-O pair at 1.53 Å,

which comes from the intercalated sulfate ion [25]. As expected, the pure GR_{SO4} only shows the sulfate S-O pair at 1.53 Å. The peaks at ~2.09 Å and 3.19 Å correspond to the octahedral coordination of Fe-O and edge sharing Fe-Fe pairs, respectively (Fig. 5b) [5]. These peaks are identical in pure GR_{SO4} and GR-BzS20, confirming that the local coordination environment of Fe within the hydroxide sheet was not changed by BzS intercalation. At R > 9.5 Å, representing distances across one or more layers, the peaks in the GR-BzS20 sample are gradually shifted to larger distances, compared to the pure GR_{SO4}. This is indicative of the difference in interlayer distances in pure GR_{SO4} and GR-BzS20. Overall, these PDF results corroborated the XRD patterns in that the BzS interacted sample contained both pure GR_{SO4} and GR with BzS in the interlayer.
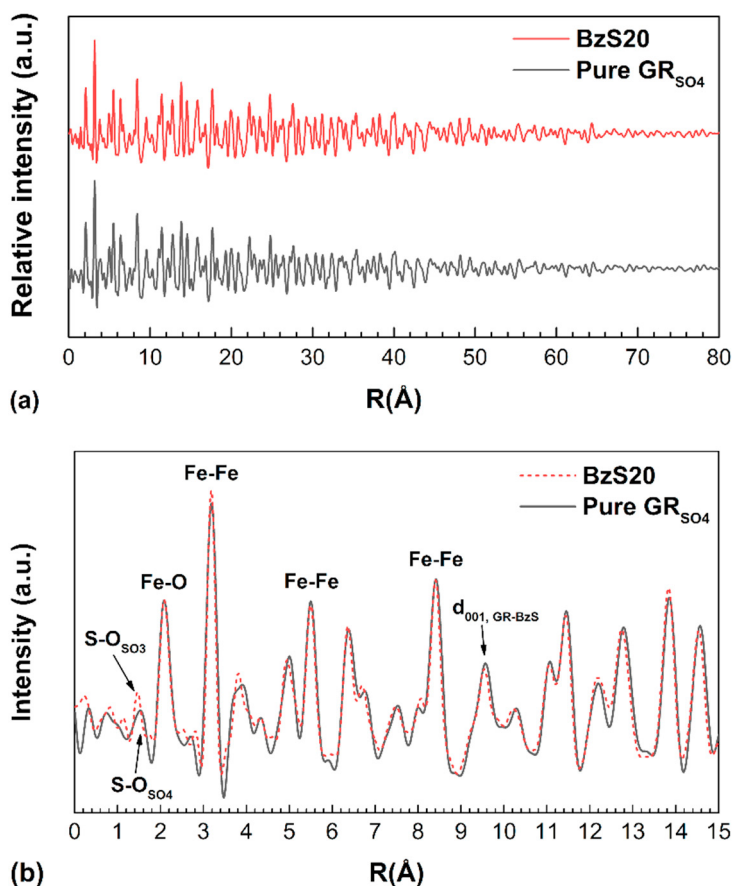

Fig. 5. (a) PDF plots of GR_{SO4} and GR-BzS20 showing similar short and medium range structure. (b) Blow-up of the PDF showing the similarities in the local structure.

3.3. Electron microscopy

TEM imaging and analyses were used to characterize the morphology, size, structure and chemical composition of the synthesized GR_{SO4} and GR-BzS particles. The micrograph of GR-BzS (Fig. 6b) revealed well-defined hexagonal plate-like particles (50-500 nm) similar to pristine GR_{SO4} (Fig. 6a). This indicates that the morphology typical of GR phases was retained even after intercalation of BzS [18]. The selected area diffraction (SAED) pattern of GR-BzS (Fig. 6b inset) exhibited the distinctive hexagonal *c*-axis spot pattern of a single crystal GR_{SO4} (Fig. 6a inset), which corresponds to the (030) and (300) lattice planes in the GR structure. EDX analyses of GR-BzS20 (Fig. 6c), collected over a hole in the carbon film of the TEM grid to avoid additional C contributions, revealed a high C peak intensity supporting the intercalation of BzS in the structure. Note that this C contribution was absent or minimal in the pure GR_{SO4} sample.
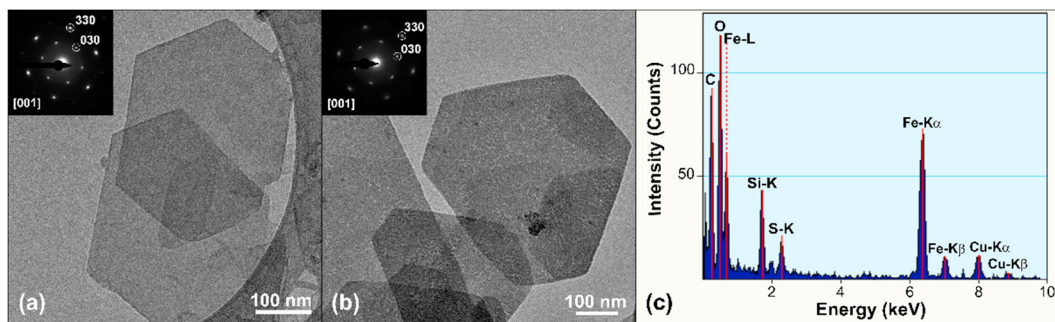
Fig. 6. TEM images of (a) GR$_{SO4}$ and (b) GR-BzS20 with SAED pattern of a single particle in inset. (c) EDX spectrum of GR-BzS20 with the prominent C peaks, and the Fe, S and O peaks marked. The Si signal comes from the use of headspace crimp bottles while Cu peaks come from the TEM grid.

3.4. Intercalation chemistry of benzene sulfonate

The possible orientation of BzS in the interlayer region of GR can be estimated based on the basal spacing (14.3 Å) derived from the XRD and PDF data (see Sections 3.1 and 3.2). The calculated diameter of the BzS molecule (8.1 Å) is substantially smaller than the interlayer spacing of GR-BzS (9.5 Å). Hence, a simple vertical dehydrated monolayer arrangement of BzS with -SO$_3$ groups facing in the same direction (Fig. 7c) previously described for Mg-Al LDHs [16] is not possible. The large interlayer spacing strongly suggest that BzS anions are likely oriented as a dehydrated monolayer with the –SO$_3$ groups facing away in alternate directions (Fig. 7a). The theoretical basal spacing for this orientation is 14.2 Å based on other organo-LDHs [26]. However, a larger basal spacing of 14.9 Å can also be obtained in a hydrated monolayer arrangement of BzS (Fig. 7b). This hydrated interlayer is also possible since water molecules can be retained in between the benzene ring and the apical –OH groups of the FeO$_6$ octahedra [26]. Hence, such interlayer arrangement cannot be completely ruled out. To confirm the orientation of BzS in the interlayer region of GR, a further study involving molecular dynamic simulations would be necessary.
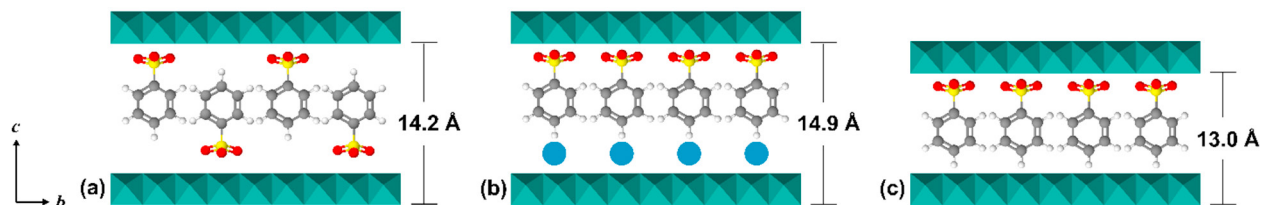

Fig. 7. Possible interlayer arrangement of BzS in the GR structure with the calculated basal spacing: (a) dehydrated monolayer arrangement with alternating sulfonate moieties facing away from each other and (b) hydrated monolayer. (c) Dehydrated BzS vertical monolayer previously described by Kameda et al. [16]. Modified from Meyn et al. [26] and Carlino et al. [27].

4. Conclusions

In this study, we have demonstrated the possibility of intercalating aromatic sulfonate into GR to produce a new organo-GR material. We have successfully intercalated BzS into the GR structure and produced a mixture of GR$_{SO4}$ and GR-BzS). On the contrary, BzDS could not be intercalated due to stearic hindrance and electrostatic repulsion. The combination of XRD, PDF and TEM imaging and spectroscopy revealed that GR-BzS incorporated the aromatic sulfonate in a monolayer arrangement without any changes in morphology or Fe bonding environment in the GR hydroxide sheets. The possible arrangement of BzS molecules in the interlayer is a dehydrated monolayer with the –SO$_3$ groups facing away in alternate directions. Our results clearly show that BzS intercalation into GR phases is feasible. It must be noted, however, that the intercalation efficiency via ion exchange is low since BzS cannot fully replace the SO$_4^{2-}$ in the interlayer. Overall, the intercalation of BzS into GR could potentially enhance the reductive

reactivity of GR for chlorinated benzenes by harnessing the enhanced hydrophobicity of the interlayer and reactivity of structural Fe(II) in GR.

Acknowledgements

References

[1] Christiansen B.C., T. Balic-Zunic, K. Dideriksen, and S.L.S. Stipp. "Identification of green rust in groundwater" *Environmental Science & Technology*, 43 (2009): 3436-41.

[2] Zegeye A., S. Bonneville, L.G. Benning, A. Sturm, D.A. Fowle, C. Jones, D.E. Canfield, C. Ruby, L.C. MacLean, S. Nomosatryo, S.A. Crowe, and S.W. Poulton. "Green rust formation controls nutrient availability in a ferruginous water column" *Geology* 40 (2012): 599-602.

[3] Usman M., J.M. Byrne, A. Chaudhary, S. Orsetti, K. Hanna, C. Ruby, A. Kappler, and S.B. Haderlein, "Magnetite and green rust: Synthesis, properties, and environmental applications of mixed-valent iron minerals", *Chemical Reviews* 118 (2018): 3251-304.

[4] Christiansen B.C., T. Balic-Zunic, P.O. Petit, C. Frandsen, S. Mørup, H. Geckeis, A. Katerinopoulou, and S.L.S. Stipp. "Composition and structure of an iron-bearing, layered double hydroxide (LDH) – Green rust sodium sulphate" *Geochimica et Cosmochimica Acta* 73 (2009): 3579-92.

[5] Christiansen B.C., K. Dideriksen, A. Katz, S. Nedel, N. Bovet, H.O. Sørensen, C. Frandsen, C. Gundlach, M.P. Andersson, and S.L.S. Stipp. "Incorporation of monovalent cations in sulfate green rust" *Inorganic Chemistry* 53: (2014) 8887-94.

[6] Lee W., B. and Batchelor. "Abiotic reductive dechlorination of chlorinated ethylenes by iron-bearing soil minerals. 2. Green rust" *Environmental Science & Technology* 36 (2002): 5348-54.

[7] Erbs M., H.C. Bruun Hansen, and C.E. Olsen. "Reductive dechlorination of carbon tetrachloride using iron(II) iron(III) hydroxide sulfate (green rust)" *Environmental Science & Technology* 33 (1999): 307-311.

[8] Mangayayam M.C., K. Diderkisen, and D.J. Tobler. "Can or cannot green rust reduce chlorinated ethenes?" *Energy Procedia* (2018): this issue.

[9] Newman S.P., and W. Jones. "Synthesis, characterization and applications of layered double hydroxides containing organic guests" *New Journal of Chemistry* 22 (1998): 105-15.

[10] Khan A.I., and D. O'Hare. "Intercalation chemistry of layered double hydroxides: recent developments and applications" *Journal of Materials Chemistry* 12 (2002): 3191-8.

[11] Rives V., and M. Angeles Ulibarri. "Layered double hydroxides (LDH) intercalated with metal coordination compounds and oxometalates" *Coordination Chemistry Reviews* 181 (1999): 61-120.

[12] Ayala-Luis K.B., D.K. Kaldor, C.B. Koch, B.W. Strobel, and H.C.B. Hansen. "Synthesis of linear alkylbenzene sulphonate intercalated iron(II) iron(III) hydroxide sulphate (green rust) and adsorption of carbon tetrachloride" *Clay Minerals* 42 (2007): 307-17.

[13] Ayala-Luis K.B., C.B. Koch, and H.C.B. Hansen. "Intercalation of linear C9–C16 carboxylates in layered Fe^{II}–Fe^{III}-hydroxides (green rust) *via* ion exchange" *Applied Clay Science* 48 (2010): 334-41.

[14] Ayala-Luis K.B., C.B. Koch, and H.C.B. Hansen. "One-pot synthesis and characterization of Fe^{II}–Fe^{III} hydroxide (green rust) intercalated with C9–C14 linear alkyl carboxylates" *Applied Clay Science* 50 (2010): 512-9.

[15] Ayala-Luis K.B., N.G.A. Cooper, C.B. Koch, and H.C.B. Hansen. "Efficient dechlorination of carbon tetrachloride by hydrophobic green rust intercalated with dodecanoate anions" *Environmental Science & Technology* 46 (2012): 3390-7.

[16] Kameda T., T. Yamazaki, and T. Yoshioka. "Preparation and characterization of Mg–Al layered double hydroxides intercalated with benzenesulfonate and benzenedisulfonate" *Microporous and Mesoporous Materials* 114 (2008): 410-5.

[17] Yu S., X. Wang, Z. Chen, J. Wang, S. Wang, T. Hayat, and X. Wang. "Layered double hydroxide intercalated with aromatic acid anions for the efficient capture of aniline from aqueous solution" *Journal of Hazardous Materials* 321 (2017): 111-20.

[18] Géhin A., C. Ruby, M. Abdelmoula, O. Benali, J. Ghanbaja, P. Refait, and J.-M.R. Génin. "Synthesis of Fe(II-III) hydroxysulphate green rust by coprecipitation" *Solid State Sciences* 4 (2002): 61-6.

[19] Hammersley A.P., S.O. Svensson, and A. Thompson. "Calibration and correction of spatial distortions in 2D detector systems" *Nuclear Instruments and Methods in Physics Research Section A: Accelerators, Spectrometers, Detectors and Associated Equipment* 346 (1994): 312-21.

[20] Hammersley A.P., S.O. Svensson, M. Hanfland, A.N. Fitch, and D. Hausermann. "Two-dimensional detector software: From real detector to idealised image or two-theta scan" *High Pressure Research* 14 (1996): 235-48.

[21] Qiu X., J.W. Thompson, and S.J.L. Billinge. "PDFgetX2: A GUI-driven program to obtain the pair distribution function from X-ray powder diffraction data" *Journal of Applied Crystallography* 37 (2004): 678.

[22] Simon L., M. François, P. Refait, G. Renaudin, M. Lelaurain, and J.-M.R. "Génin, Structure of the Fe(II-III) layered double hydroxysulphate green rust two from Rietveld analysis" *Solid State Sciences* 5 (2003): 327-34.

[23] Sasaki T., M. Watanabe, Y. Michiue, Y. Komatsu, F. Izumi, S. Takenouchi. "Preparation and acid-base properties of a protonated titanate with the lepidocrocite-like layer structure" *Chemistry of Materials* 7 (1995): 1001-7.

[24] Le Bail A. "Monte Carlo indexing with McMaille" *Powder Diffraction* 19 (2004): 249-54.

[25] Shannon R.D. "Revised effective ionic radii and systematic studies of interatomic distances in halides and chalcogenides" *Acta Crystallographica Section A* 32 (1976): 751-67.

[26] Meyn M., K. Beneke, and G. Lagaly. "Anion-exchange reactions of layered double hydroxides" *Inorganic Chemistry* 29 (1990): 5201-7.

[27] Carlino S. "The intercalation of carboxylic acids into layered double hydroxides: a critical evaluation and review of the different methods" *Solid State Ionics* 98 (1997): 73-84.